Drug Delivery

DOI: 10.1002/ange.201300958

Glucose- and pH-Responsive Controlled Release of Cargo from Protein-Gated Carbohydrate-Functionalized Mesoporous Silica Nanocontainers**

*Shanshan Wu, Xuan Huang, and Xuezhong Du**

To improve the therapeutic efficacy and to reduce adverse side effects of drugs, one strategy is to design a target-specific drug-delivery system that can transport an effective dosage of drug molecules to the targeted cells and tissues on time.[1] For drug-delivery systems, no premature release and stimuli-responsive controlled release of the pharmaceutical cargo are two very important prerequisites that impact the therapeutic efficacy and cytotoxicity of the drug delivery.[2] Mesoporous silica nanoparticles (MSNs) have been used in delivery systems as nanocontainers because of their excellent biocompatibility, high surface areas, large pore volumes, uniform and tunable pore sizes, and a great diversity of surface functionalization,[3] in comparison with traditional delivery systems, which mainly depend on simple diffusion or degradation of the nanocarriers.[1] A variety of MSN-based controlled-release systems[4] have been developed using nanoparticles (CdS,[5a] Fe_3O_4,[5b] Au,[5c–f] and ZnO[5g]), macrocyclic compounds (cyclodextrins[6a–e] and cucurbiturils[6f–k]), dendrimers,[7] polymers,[8] and biomacromolecules (proteins[9] and DNA[2,5c,10]) responsive to various external stimuli, such as pH,[5e,6a,f–i,10b] competitive binding,[6i,j,8a] redox,[8,9] light,[5e,6k,7,8a] and enzymes.[2,6c,d,j,11] Despite the significant progress that has been made, the direct use of biomolecules as gatekeepers is still in its infancy. Based on the biotin–avidin complex, the strongest noncovalent interaction found in nature, with a binding constant of 10^{13}–10^{15} $L\,mol^{-1}$, avidin-gated MSN nanocontainers have been constructed for protease- and temperature (90 °C)-responsive controlled release through proteolytic digestion and protein denaturation.[12] Based on an antibody and hapten interaction, antibody-gated MSN nanocontainers have been used for competitive-binding-driven controlled release.[13] Similarly, glucose oxidase-gated MSN nanocontainers were also designed on the basis of an enzyme-inhibition mechanism,[14] and the release could be triggered by glucose at very low concentrations (3.3×10^{-4} $mmol\,L^{-1}$). Biomacromolecule-gated MSN delivery systems are highly desirable for practical applications in disease-related environments.

Herein, we report the controlled release of cargo from novel protein-gated carbohydrate-functionalized MSN nanocontainers. Carbohydrate–protein interactions play an important role in a variety of cellular processes including cell differentiation and adhesion, inflammation, metastasis, and immune response.[15] However, monovalent carbohydrate–protein interactions are inherently weak, with a binding constant of 10^3–10^4 $L\,mol^{-1}$,[16] and the interaction strength and specificity can be improved with multivalent interactions or several simultaneous binding events with a binding constant of 10^6–10^7 $L\,mol^{-1}$ or higher.[16] Concanavalin A (Con A, pI = 4.5–5.5, a tetrameric form under physiological conditions,[17] $3.9\times4.0\times4.2$ nm for the tetramer)[17b] is capable of specifically binding mannose and glucose epitopes in the presence of Mn^{2+} and Ca^{2+} ions but with higher affinity for mannose.[17] Carbohydrate-functionalized nanoparticles and vesicles have been used for protein recognition and sensing through the multivalent carbohydrate–protein interactions.[18] Herein, MSNs were functionalized with mannose ligands at optimized surface densities, tight Con A nanogates were then constructed using multivalent carbohydrate–protein interactions to encapsulate the cargo within the pores, and the cargo was released by introducing an acidic environment, such as is found in tumor cells and inflammatory tissue. pH-controlled drug delivery could be important for cancer therapy, while also reducing side effects.[19] In addition, the drug could also be released by competitive binding of glucose when the normal blood-glucose concentration becomes elevated, which would have potential applications for diabetes therapy.

Controlled release from Con A-gated MSN nanocontainers is shown in Scheme 1. MCM-41-type MSNs with cylindrical channels were used as the nanocontainers. Mercapto-terminated mannose derivatives were synthesized (Supporting Information, Scheme S1), reacted with alkenyl-terminated silanes using a thiol–ene click reaction (Scheme S2), and finally the external surfaces of MCM-41 were functionalized with mannose epitopes. Subsequent capping with Con A encapsulated the cargo within the pores through the multivalent carbohydrate–protein interactions. Rhodamine 6G (Rh6G) was selected as a model drug for convenient detection of the release, because its fluorescence emission remains unchanged not only in the presence of Ca^{2+}, Mn^{2+}, and Con A but also with a change of pH from 7.4 to 1.5 (Figure S1). Con A is a metalloprotein and requires Ca^{2+} and a transition metal ion such as Mn^{2+} to bind to carbohydrates.[16] The carbohydrate-binding activity is abolished upon

[*] S. Wu, X. Huang, Prof. Dr. X. Du
Key Laboratory of Mesoscopic Chemistry (Ministry of Education), School of Chemistry and Chemical Engineering
Nanjing University, Nanjing 210093 (China)
E-mail: xzdu@nju.edu.cn

[**] This work was supported by the National Natural Science Foundation of China (21273112) and the Natural Science Foundation of Jiangsu Province (BK2012719).

Supporting information for this article is available on the WWW under http://dx.doi.org/10.1002/anie.201300958.

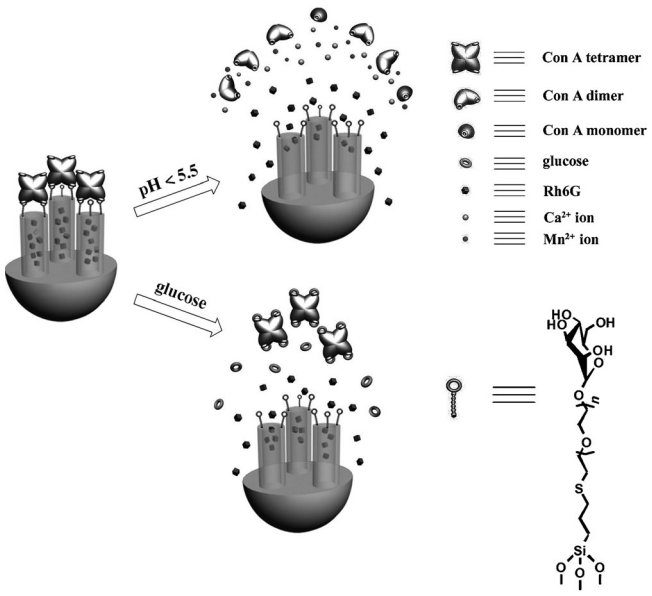

Scheme 1. Illustration of the controlled release of cargo from Con A-gated mannose-functionalized MSN nanocontainers in response to changes in pH value and glucose concentration.

removal of these metal ions by dialysis under acidic conditions, on the other hand, Con A exists as a dimer and/or monomer below pH 5.5. We would expect the protein nanogates to release their cargo either upon exposure to acidic environments or by competitive binding of glucose.

MCM-41 materials were synthesized using the base-catalyzed sol-gel method, and then the cetyltrimethylammonium bromide (CTAB) templates were removed. From the scanning electron microscope (SEM) and transmission electron microscope (TEM) images of MCM-41 (Figure S2), MSNs were 110 ± 10 nm in diameter and contained hexagonally arranged pores. Upon modification of mannose-terminated silane with an oligo(ethylene glycol) (OEG) spacer **S1**, the mannose-functionalized MSNs were referred to as **MS1. MS1-1**, **MS1-2**, and **MS1-3** represented MSNs functionalized with **S1** at different surface densities, which were determined by thermogravimetric analysis to be 0.137, 0.284, and 0.410 mmol g^{-1} SiO_2 (Figure S3), respectively. However, the SEM and TEM images of **MS1** and the Con A-capped **MS1** series (Figure S4) did not show significant differences from those of MCM-41, probably owing to the relatively small dimensions of **S1** and Con A and the conditions under which the microscopic images were taken.

Solid-state NMR spectra of **MS1-1**, **MS1-2**, and **MS1-3** clearly confirm the functionalization of the surface with mannose ligands. In the solid-state ^{13}C NMR spectra (Figure S5), two weak signals at $\delta = 31.24$ ppm and 35.52 ppm were ascribed to the resonances of the two carbon atoms directly connected to the sulfur atom, which confirms the success of the thiol–ene click reaction. In the solid-state ^{29}Si NMR spectra (Figure S6), the two resonances at $\delta = -50.56$ ppm and -56.51 ppm corresponded to the organosilica T^1 and T^2 species, assigned to $[RSiOSi(OH)_2]$ and $[RSi(OSi)_2OH]$,[20,21] respectively. These two peaks resulted from silicon atoms covalently bound to the organic substituents. The organosilica species underwent a gradual change from T^2 to T^1 with the increase of the surface density of mannose. Combination of the ^{13}C and ^{29}Si NMR spectra confirmed that the mannose-terminated silanes were covalently immobilized on the MCM-41 surfaces.

FTIR spectroscopy was further used to characterize the functionaliztion of the MSN surface and protein capping (Figure S7). The removal of surfactants was confirmed by the disappearance of three strong bands at 2923, 2853, and 1478 cm^{-1}, owing to the CH_2 stretching and bending vibrations of CTAB. With **MS1-1**, **MS1-2**, and **MS1-3**, the weak bands at 2955 and 2855 cm^{-1} were observed from the C–H stretching vibrations, while corresponding C–O stretching bands could not be distinguished from the strong Si–O–Si stretching bands at 1230–1000 cm^{-1}. Upon capping with Con A (without Rh6G loading for clarity), strong amide I and amide II bands at 1648 and 1540 cm^{-1} were observed, but the amount of Con A was highest at the middle surface density of mannose ligands (**MS1-2**). Further thermogravimetric analysis indicated that the maximum weight-loss percentage between the **MS1** and Con A-capped **MS1** series was observed for **MS1-2** (Figure S8), which further demonstrates that the amount of Con A on **MS1-2** was the highest, which is favorable for tight closure of the MSN pores. It is known that specific mannose–Con A interactions are achieved by the access of the carbohydrate ligands to protein binding pockets in the presence of Ca^{2+} and Mn^{2+} ions. Low surface-ligand density limits multivalent protein binding, whereas high surface density could result in steric crowding of the neighboring ligands, which would be unfavorable to multivalent protein binding. It has been shown that the amount of specifically bound proteins is closely related to the surface density and spatial arrangement of the carbohydrate ligands and is determined by the balance between these two factors.[16c,d] The zeta potential values of MCM-41, **MS1-2**, and Con A-capped **MS1-2** were -51.9, -33.4, and -13.1 mV, respectively (Figure S9a), and the hydrodynamic diameters of the corresponding nanoparticles were 112 ± 7, 128 ± 10, and 219 ± 15 nm, respectively (Figure S9b). These indicate that the Con A-gated **MS1-2** with the highest protein loading was well-dispersed in aqueous solution without significant aggregation, taking into account the easily hydrated OEG-linked mannose ligands and the dimensions and isoelectric point of Con A (Type V, pI = 4.7).

The small-angle powder X-ray diffraction (XRD) patterns of MCM-41 after CTAB removal exhibited three well-resolved reflections, indexed as (100), (110), and (200)[22] (Figure S10), which is typical of a hexagonal mesoporous structure. **MS1-1**, **MS1-2**, and **MS1-3** also showed similar XRD patterns to MCM-41, which indicates that the functionalized mannose epitopes (with different surface densities) did not influence the mesoporous structure of the silica matrix. However, none of the three peaks was detectable after loading with Rh6G (loading of 0.183 mmol g^{-1} SiO_2, as determined by fluorescence spectroscopy) and capping with Con A, owing to an effect from the filled pores.

The nitrogen adsorption–desorption isotherms of MCM-41 showed typical type IV curves with a surface area of 1093 $m^2 g^{-1}$ and an average pore size of 2.9 nm (Figure S11

and Table S1). **MS1-1**, **MS1-2**, and **MS1-3** decreased in surface area and pore size with an increase in surface density of mannose ligands, because the surface area was considerably reduced and the pore was filled upon loading of Rh6G and subsequent capping with Con A (Figure S12).

Fluorescence spectroscopy was used to check for any premature release of Rh6G from Con A-gated **MS1** systems in the buffer solution (pH 7.4) before the pH trigger was added (Figure 1 a). The fluorescence emission of the Con A-gated **MS1** systems remained low and almost unchanged after two hours, which indicated that the cargo remained entrapped in the pores. The Con A-gated **MS1** systems showed a good

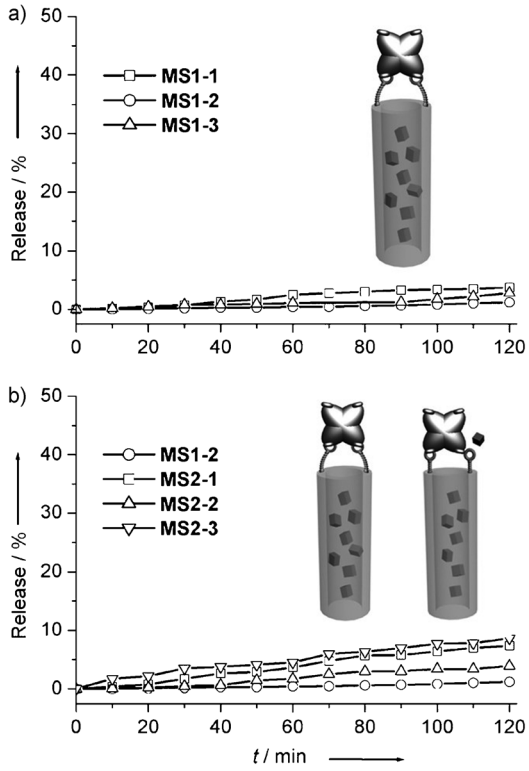

Figure 1. Release profiles of Rh6G from Con A-gated mannose-functionalized MSNs with different surface ligand densities in tris-HCl buffer solutions (pH 7.4): a) **MS1** series; b) **MS2** series together with **MS1-2** for comparison. Drawings show retention of cargo (a) and slow release of some cargo (b) from the MSN pores.

blocking effect with minimal premature release of the dye, especially for the Con A-gated **MS1-2**. Similarly, MSNs were functionalized with mannose-terminated silanes without an OEG spacer (**S2**) at different surface densities (0.164, 0.286, and 0.443 mmol g^{-1} SiO_2; Figure S13) and were accordingly referred to as **MS2-1**, **MS2-2**, and **MS2-3** (Figure 1 b). The FTIR spectra (Figure S14), small-angle XRD patterns (Figure S15), and nitrogen adsorption–desorption isotherms under different conditions for **MS2** were recorded (Figures S16,S17 and Table S2). The Rh6G-loaded, Con A-gated **MS2** systems showed slight leakage over time before the pH trigger was added, in comparison with the Con A-gated **MS1** systems. The carbohydrate ligands protruding from the biocompatible silica surfaces with a suitable spatial arrangement enhanced protein binding. The long and flexible OEG spacers played an important role in adjusting the local spatial arrangement of the ligands and allowed for better binding of the ligands for multivalent carbohydrate–protein interactions, in contrast to the short linkers used in other MSN-based delivery systems.[6f]

Upon decreasing the pH of the buffer, the fluorescence emission of the Con A-gated **MS1-2** system significantly increased (Figure 2), which indicates that the protein nanogates opened and the cargo was released from the MSN pores. The efficiency of release significantly increased from pH 7.4 to 5.5, and additionally to pH 3.5 and 1.5. Under acidic

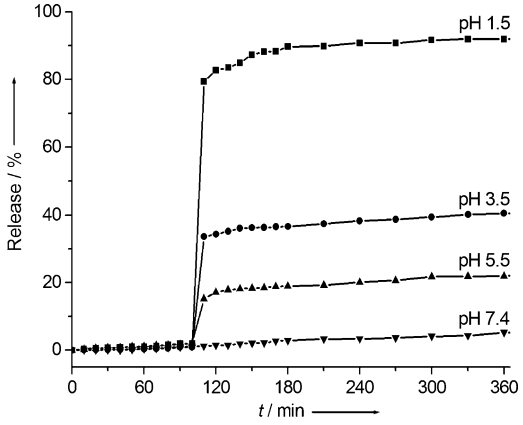

Figure 2. Release profiles of Rh6G from Con A-gated **MS1-2** at different pH values.

conditions, Ca^{2+} and Mn^{2+} ions were dialyzed out of the protein binding pockets, resulting in removal of the Con A proteins from the **MS1-2** surface, in addition, the Con A tetramers disassociated into dimers and monomers below pH 5.5. Both of these factors caused the protein nanogates to open and release their cargo to different extents dependent on the pH value. The amount of cargo released could be controlled in small steps with the continued stepwise decrease in pH value of the buffer (Figure S18). After the release of cargo at pH 1.5, the delivery system showed the same FTIR spectrum as **MS1-2** confirming the disappearance of the amide I and amide II bands of the proteins (Figure S7); the SEM and TEM images were nearly identical to those of **MS1-2** without visible morphological changes or pore collapse (Figure S19); the XRD reflection peaks reappeared but with reduced intensities (Figure S10); the surface area returned to 642 $m^2 g^{-1}$ from 51 $m^2 g^{-1}$, and the pore diameter was restored to the original size of 2.5 nm of **MS1-2** (Figure S12 and Table S1). All of these changes indicate that the protein nanogates of the delivery system opened and the cargo was released under acidic conditions, although there was a small amount of dye retained in the pores.

Glucose is capable of specifically binding Con A in the presence of Mn^{2+} and Ca^{2+} ions but with lower binding affinity than mannose. In the presence of glucose, the fluorescence emission of the Con A-gated **MS1-2** system gradually increased with increasing glucose concentration

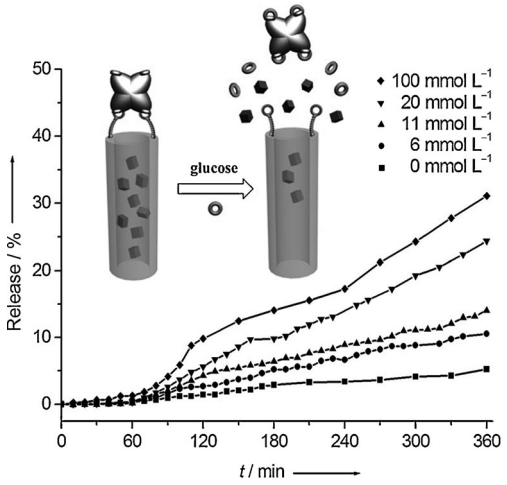

Figure 3. Release profiles of Rh6G from Con A-gated **MS1**-**2** in the presence of different concentrations of glucose in tris-HCl buffer solution (pH 7.4).

because of competitive binding of glucose to the proteins which drove the removal of proteins and the controlled release of cargo (Figure 3). The normal concentration ranges of glucose are 4–7 mmol L^{-1} before a meal and less than 10 mmol L^{-1} about 1.5 hours after a meal. Thus, glucose in the normal range could not trigger a significant release of cargo because glucose is a weak competitor in comparison with mannose, and it is difficult for glucose at low concentrations to disrupt the multivalent mannose–Con A interactions. On the other hand, high concentrations of glucose could give rise to a slow release of cargo from the MSN pores, and the amount of cargo released would increase with time for application in a sustained release system. The mechanism of controlled release by competitive binding is different from that of the pH-responsive release. It is clear that the Con A-gated **MS1** systems have promise for applications in site-specific drug release, relevant to tumors and diabetes.

In summary, Con A-gated mannose-functionalized MSN delivery systems were constructed for the controlled release of drugs. The Con A tetramers specifically bound the functionalized mannose epitopes through multivalent carbohydrate–protein interactions to encapsulate cargo within the MSN pores. The long and flexible spacers linked with the mannose ligands played an important role in adjusting the local spatial arrangement of the ligands to favor multivalent protein binding, as did the surface density of the ligands. The optimized protein-gated delivery systems showed minimal premature release of cargo. The protein nanogates could be opened either by decreasing the pH value of the buffer or by competitive binding of glucose at high concentrations, releasing the cargo from the MSN pores on demand. These Con A-gated MSN delivery systems are promising for in vivo applications of site-specific drug release for the treatment of tumors and diabetes.

Received: February 3, 2013
Published online: April 15, 2013

Keywords: carbohydrates · controlled release · drug delivery · molecular devices · proteins

[1] I. I. Slowing, J. L. Vivero-Escoto, C.-W. Wu, V. S.-Y. Lin, *Adv. Drug Delivery Rev.* **2008**, *60*, 1278 – 1288.
[2] C. Chen, J. Geng, F. Pu, X. Yang, J. Ren, X. Qu, *Angew. Chem.* **2011**, *123*, 912 – 916; *Angew. Chem. Int. Ed.* **2011**, *50*, 882 – 886.
[3] a) Y. Liu, W. Zhang, T. Pinnavaia, *Angew. Chem.* **2001**, *113*, 1295 – 1298; *Angew. Chem. Int. Ed.* **2001**, *40*, 1255 – 1258; b) Y. Han, D. Li, L. Zhao, F. Xiao, *Angew. Chem.* **2003**, *115*, 3761 – 3765; *Angew. Chem. Int. Ed.* **2003**, *42*, 3633 – 3637.
[4] a) M. W. Ambrogio, C. R. Thomas, Y.-L. Zhao, J. I. Zink, J. F. Stoddart, *Acc. Chem. Res.* **2011**, *44*, 903 – 913; b) P. Yang, S. Gai, J. Lin, *Chem. Soc. Rev.* **2012**, *41*, 3679 – 3698; c) Y.-W. Yang, *Med. Chem. Commun.* **2011**, *2*, 1033 – 1049.
[5] a) C.-Y. Lai, B. G. Trewyn, D. M. Jeftinija, K. Jeftinija, S. Xu, S. Jeftinija, V. S.-Y. Lin, *J. Am. Chem. Soc.* **2003**, *125*, 4451 – 4459; b) S. Giri, B. G. Trewyn, M. P. Stellmaker, V. S.-Y. Lin, *Angew. Chem.* **2005**, *117*, 5166 – 5172; *Angew. Chem. Int. Ed.* **2005**, *44*, 5038 – 5044; c) F. Torney, B. G. Trewyn, V. S.-Y. Lin, K. Wang, *Nat. Nanotechnol.* **2007**, *2*, 295 – 300; d) J. L. Vivero-Escoto, I. I. Slowing, C.-W. Wu, V. S.-Y. Lin, *J. Am. Chem. Soc.* **2009**, *131*, 3462 – 3463; e) E. Aznar, M. D. Marcos, R. Martínez-Máñez, F. Sancenón, J. Soto, R. Casasús, P. Amorós, C. Guillem, *J. Am. Chem. Soc.* **2009**, *131*, 6833 – 6843; f) R. Liu, Y. Zhang, X. Zhao, A. Agarwal, L. J. Mueller, P. Feng, *J. Am. Chem. Soc.* **2010**, *132*, 1500 – 1501; g) F. Muhammad, M. Guo, W. Qi, F. Sun, A. Wang, Y. Guo, G. Zhou, *J. Am. Chem. Soc.* **2011**, *133*, 8778 – 8781.
[6] a) C. Park, K. Oh, S. C. Lee, C. Kim, *Angew. Chem.* **2007**, *119*, 1477 – 1479; *Angew. Chem. Int. Ed.* **2007**, *46*, 1455 – 1457; b) C. Park, K. Lee, C. Kim, *Angew. Chem.* **2009**, *121*, 1301 – 1304; *Angew. Chem. Int. Ed.* **2009**, *48*, 1275 – 1278; c) C. Park, H. Kim, S. Kim, C. Kim, *J. Am. Chem. Soc.* **2009**, *131*, 16614 – 16615; d) K. Patel, S. Angelos, W. R. Dichtel, A. Coskun, Y.-W. Yang, J. I. Zink, J. F. Stoddart, *J. Am. Chem. Soc.* **2008**, *130*, 2382 – 2383; e) D. P. Ferris, Y.-L. Zhao, N. M. Khashab, H. A. Khatib, J. F. Stoddart, J. I. Zink, *J. Am. Chem. Soc.* **2009**, *131*, 1686 – 1688; f) S. Angelos, Y. Yang, K. Patel, J. F. Stoddart, J. I. Zink, *Angew. Chem.* **2008**, *120*, 2254 – 2258; *Angew. Chem. Int. Ed.* **2008**, *47*, 2222 – 2226; g) S. Angelos, N. M. Khashab, Y. Yang, A. Trabolsi, H. A. Khatib, J. F. Stoddart, J. I. Zink, *J. Am. Chem. Soc.* **2009**, *131*, 12912 – 12914; h) S. Angelos, Y. Yang, N. M. Khashab, J. F. Stoddart, J. I. Zink, *J. Am. Chem. Soc.* **2009**, *131*, 11344 – 11346; i) J. Liu, X. Du, *J. Mater. Chem.* **2010**, *20*, 3642 – 3649; j) J. Liu, X. Du, X. Zhang, *Chem. Eur. J.* **2011**, *17*, 810 – 815; k) Y.-L. Sun, B.-J. Yang, S. X.-A. Zhang, Y.-W. Yang, *Chem. Eur. J.* **2012**, *18*, 9212 – 9216.
[7] E. Aznar, R. Casasús, B. García-Acosta, M. D. Marcos, R. Martínez-Máñez, F. Sancenón, J. Soto, P. Amorós, *Adv. Mater.* **2007**, *19*, 2228 – 2231.
[8] a) R. Liu, Y. Zhang, P.-Y. Feng, *J. Am. Chem. Soc.* **2009**, *131*, 15128 – 15129; b) R. Liu, X. Zhao, T. Wu, P. Feng, *J. Am. Chem. Soc.* **2008**, *130*, 14418 – 14419.
[9] a) Y. Zhao, B. G. Trewyn, I. I. Slowing, V. S.-Y. Lin, *J. Am. Chem. Soc.* **2009**, *131*, 8398 – 8400; b) Z. Luo, K. Cai, Y. Hu, L. Zhao, P. Liu, L. Duan, W. Yang, *Angew. Chem.* **2011**, *123*, 666 – 669; *Angew. Chem. Int. Ed.* **2011**, *50*, 640 – 643.
[10] a) E. Climent, R. Martínez-Máñez, F. Sancenón, M. D. Marcos, J. Soto, A. Maquieira, P. Amorós, *Angew. Chem.* **2010**, *122*, 7439 – 7441; *Angew. Chem. Int. Ed.* **2010**, *49*, 7281 – 7283; b) C. Chen, F. Pu, Z. Huang, Z. Liu, J. Ren, X. Qu, *Nucleic Acids Res.* **2011**, *39*, 1638 – 1644.
[11] A. Popat, B. P. Ross, J. Liu, S. Jambhrunkar, F. Kleitz, S. Z. Qiao, *Angew. Chem.* **2012**, *124*, 12654 – 12657; *Angew. Chem. Int. Ed.* **2012**, *51*, 12486 – 12489.

[12] A. Schlossbauer, J. Kecht, T. Bein, *Angew. Chem.* **2009**, *121*, 3138 – 3141; *Angew. Chem. Int. Ed.* **2009**, *48*, 3092 – 3095.
[13] E. Climent, A. Bernardos, R. Martínez-Máñez, A. Maquieira, M. D. Marcos, N. Pastor-Navarro, R. Puchades, F. Sancenón, J. Soto, P. Amorós, *J. Am. Chem. Soc.* **2009**, *131*, 14075 – 14080.
[14] M. Chen, C. Huang, C. He, W. Zhu, Y. Xu, Y. Lu, *Chem. Commun.* **2012**, *48*, 9522 – 9524.
[15] C. R. Bertozzi, L. L. Kiessling, *Science* **2001**, *291*, 2357 – 2364.
[16] a) E. A. Smith, W. D. Thomas, L. L. Kiessling, R. M. Corn, *J. Am. Chem. Soc.* **2003**, *125*, 6140 – 6148; b) P.-H. Liang, S.-K. Wang, C.-H. Wong, *J. Am. Chem. Soc.* **2007**, *129*, 11177 – 11184; c) H. Zheng, X. Du, *J. Phys. Chem. B* **2009**, *113*, 11330 – 11337; d) H. Zheng, X. Du, *Biochim. Biophys. Acta* **2013**, *1828*, 792 – 800.
[17] a) K. D. Hardman, C. F. Ainsworth, *Biochemistry* **1972**, *11*, 4910 – 4949; b) J. W. Becker, G. N. Reeke, Jr., B. A. Cunningham, G. M. Edelman, *Nature* **1976**, *259*, 406 – 409; c) G. M. Edelman, B. A. Cunningham, G. N. Reeke, Jr., J. W. Becker, M. J. Waxdal, J. L. Wang, *Proc. Natl. Acad. Sci. USA* **1972**, *69*, 2580 – 2584.
[18] a) E. Mahon, T. Aastrup, M. Barboiu, *Chem. Commun.* **2010**, *46*, 2441 – 2443; b) J.-F. Nierengarten, J. Iehl, V. Oerthel, M. Holler, B. M. Illescas, A. Muñoz, N. Martín, J. Rojo, M. Sánchez-Navarro, S. Cecioni, S. Vidal, K. Buffet, M. Durka, S. P. Vincent, *Chem. Commun.* **2010**, *46*, 3860 – 3862; c) X. Wang, O. Ramström, M. Yan, *Anal. Chem.* **2010**, *82*, 9082 – 9089; d) O. Norberg, I. H. Lee, T. Aastrup, M. Yan, O. Ramström, *Biosens. Bioelectron.* **2012**, *34*, 51 – 56.
[19] J. Zhu, L. Liao, X. Bian, J. Kong, P. Yang, B. Liu, *Small* **2012**, *8*, 2715 – 2720.
[20] a) M. Jia, A. Seifert, W. R. Thiel, *Chem. Mater.* **2003**, *15*, 2174 – 2180; b) M. Jia, A. Seifert, M. Berger, H. Giegengack, S. Schulze, W. R. Thiel, *Chem. Mater.* **2004**, *16*, 877 – 882.
[21] a) D. W. Sindorf, G. E. Maciel, *J. Am. Chem. Soc.* **1983**, *105*, 3767 – 3776; b) E. Lindner, T. Schneller, F. Auer, H. A. Mayer, *Angew. Chem.* **1999**, *111*, 2288 – 2309; *Angew. Chem. Int. Ed.* **1999**, *38*, 2154 – 2174.
[22] C. T. Kresge, M. E. Leonowicz, W. J. Roth, J. C. Vartuli, J. S. Beck, *Nature* **1992**, *359*, 710 – 712.